Thionation Enhances the Electron Mobility of Perylene Diimide for High Performance n-Channel Organic Field Effect Transistors

Andrew J. Tilley, Chang Guo, Mark B. Miltenburg, Tyler B. Schon, Han Yan, Yuning Li, and Dwight S. Seferos**

Perylene diimides (PDIs) are one of the most widely studied n-type materials, showing great promise as electron acceptors in organic photovoltaic devices and as electron transport materials in n-channel organic field effect transistors. Amongst the well-established chemical modification strategies for increasing the electron mobility of PDI, substitution of the imide oxygen atoms with sulfur, known as thionation, has remained largely unexplored. In this work, it is demonstrated that thionation is a highly effective means of enhancing the electron mobility of a bis-*N*-alkylated PDI derivative. Successive oxygen–sulfur substitution increases the electron mobility such that the fully thionated derivative (S4) has an average mobility of 0.16 $cm^2 V^{-1} s^{-1}$. This is two orders of magnitude larger than the nonthionated parent compound (P), and is achieved by solution deposition and without thermal or solvent vapor annealing. A combination of atomic force microscopy and 2D wide angle X-ray scattering experiments, together with theoretical modeling of charge transport efficiency, is used to explain the strong positive correlation observed between electron mobility and degree of thionation. This work establishes thionation as a highly effective means of enhancing the electron mobility of PDI, and provides motivation for the development of thionated PDI derivatives for organic electronics applications.

1. Introduction

Solution processed organic field effect transistors (OFETs) are necessary to realize low cost, flexible and large scale electronic devices. For organic photovoltaic devices (OPVs) and complementary logic circuits, high mobility hole and electron transporting materials (so-called p- and n-type materials) are required to achieve performance comparable to the benchmark inorganic technologies. While excellent progress has been made in the development of high mobility p-type materials,[1] their n-type counterparts have lagged behind primarily due to their inherent atmospheric sensitivity and the smaller subset of molecular scaffolds available for their synthesis.[2]

Perylene diimide (PDI) derivatives are amongst the most widely studied n-type materials as they can be readily functionalized, have tunable electronic properties, possess high molar absorption coefficients in the visible region of the electromagnetic spectrum, are thermally stable, and can form ordered nanostructures conducive to charge transport.[3] The ability to functionalize the perylene core (at the so-called bay and headland positions) and the imide nitrogens with a variety of substituents has led to a vast number of polymeric and small molecule architectures, including alternating copolymers,[4] terpolymers,[5] fused ring systems,[6] molecular dimers and trimers,[7] and organometallic complexes.[8] Such elaborate architectures are being applied in a variety of applications, including as alternatives to fullerene derivatives in OPVs,[9] as triplet acceptors for singlet fission,[10] as singlet fission materials,[11] and as electron transport materials in organic light-emitting diodes[12] and OFETs.[13–15]

For n-channel OFETs it is necessary for the organic semiconductor to possess a high electron affinity [low lowest unoccupied molecular orbital (LUMO) energy] to facilitate electron injection and transport, and for it to form ordered crystalline domains that facilitate efficient charge transport to the electrodes. This is particularly important in OFETs since the precise solid state packing arrangement and molecular orientation with respect to the dielectric surface can have a profound influence on both short and long range charge transport efficiency.[16] PDI derivatives are thus attractive candidates for n-channel OFETs

Dr. A. J. Tilley, M. B. Miltenburg, T. B. Schon, Dr. H. Yan, Prof. D. S. Seferos
Lash Miller Chemical Laboratories
Department of Chemistry
University of Toronto
80 St. George Street, Toronto,
Ontario M5S 3H6, Canada
E-mail: dseferos@chem.utoronto.ca
C. Guo, Prof. Y. Li
Department of Chemical Engineering
and Waterloo Institute for Nanotechnology (WIN)
University of Waterloo
200 University Ave West
Waterloo, Ontario N2L 3G1, Canada
E-mail: yuning.li@waterloo.ca

DOI: 10.1002/adfm.201500837

since the bay and headland positions can be functionalized with a variety of electron withdrawing groups (such as CN,[17] F,[18] Cl,[19] and perfluoroalkyl[20]) to lower the LUMO energy, while substituents at the imide nitrogen positions can be used to optimize solid state packing and also to lower the LUMO energy (particularly in the case of fluorinated substituents).[21] This synthetic versatility has seen electron mobilities of 3.5 $cm^2\ V^{-1}\ s^{-1}$ reached in a vapor deposited film of an *N,N′*-tridecyl PDI derivative following thermal annealing,[22] with linear *N*-alkyl sidechains typically producing the best OFET performance.[23]

A number of PDI small molecule derivatives have been tested for n-channel OFETs, and the reader is referred to the following comprehensive reviews.[14,15,24] Two critical points emerge from these exhaustive surveys: the first is that the design of new PDI small molecule derivatives has primarily focused on functionalizing the perylene core and/or imide nitrogens. New synthetic protocols for functionalizing PDI that modify the optoelectronic and materials properties would allow for the development of yet more diverse architectures. The second key point is that the highest mobility devices have generally been achieved by thermal deposition of the semiconducting layer followed by post-deposition treatment (such as thermal or solvent vapor annealing), to create a favorable film morphology for charge transport. This potentially hinders commercial applicability since thermal processing techniques are energy intensive and thus not advantageous for large scale production of OFETs.

Recently, we showed that the optoelectronic properties and solid state molecular packing of a bis-*N*-alkylated PDI derivative could be altered by thionation of the imide carboxyl groups.[25] Through successive oxygen–sulfur atomic substitution we observed a sequential increase in electron affinity, and solid-state optical properties indicative of strong π–π interactions (H-aggregate formation) in as-cast films of these materials. Motivated by these results, we herein report the performance of solution processed OFETs based on a family of thionated PDIs. We find that high electron mobilities can be obtained without the need for thermal or solvent vapor annealing, which is in contrast to the majority of high performance OFETs that utilize a PDI-based semiconductor. A combination of atomic force microscopy (AFM), 2D wide angle X-ray scattering (2D-WAXS) experiments and theoretical calculations are used to investigate molecular packing and charge transport in these systems. We find that the average electron mobility increases with the degree of thionation such that **S4** has the highest average mobility of the materials studied (0.16 $cm^2\ V^{-1}\ s^{-1}$). This is attributed to a sequential increase in electron affinity and intermolecular electron transfer efficiency with degree of thionation, together with solid-state properties conducive for efficient long-range charge transport in films of the thionated derivatives. Our results show that any degree of thionation improves the electron mobility of PDI, opening the door for the development of new thionated PDI derivatives for organic electronics applications.

2. Results and Discussion

2.1. Transistor Performance

The PDIs investigated in this work are shown in **Figure 1** and Figure S1, Supporting Information. The synthesis and photophysical properties of these compounds have been reported in a previous study.[25] To evaluate the charge transport properties of the PDIs, bottom gate, bottom contact OFETs were fabricated on n^{++} Si/SiO_2 substrates with patterned gold source and drain electrodes. The Si/SiO_2 surface was pretreated with trichlorododecylsilane (TDS), which forms a surface monolayer that is reported to reduce charge trapping at the SiO_2/semiconductor interface,[26] and can orient the molecules in a favorable edge-on configuration for charge transport. PDI thin films were spin coated from 10 mg mL^{-1} chloroform solutions at a spin speed of 6000 rpm for **P** and 3000 rpm for the thionated derivatives for 60 s. Complete removal of the solvent was achieved by warming the devices for 10 min at 30 °C immediately following spin coating. All devices were fabricated and tested in a nitrogen-filled glove box at ambient temperature.

Output and transfer curves for the champion devices show that each derivative displays n-type characteristics (Figure 1 and Figure S1, Supporting Information). Electron mobilities (μ_e) were calculated in the saturation regime at a drain–source voltage (V_{DS}) of 100 V, and were found to correlate well with increasing electron affinity such that **S4** displays the highest average electron mobility of the materials studied (μ_e = 0.16 $cm^2\ V^{-1}\ s^{-1}$, $I_{on/off} = \approx 3 \times 10^3$) (**Table 1**) (**Figure 2**). In comparison, the parent compound (**P**) has an average electron mobility of 6.9×10^{-4} $cm^2\ V^{-1}\ s^{-1}$ and on/off ratio of $\approx 10^3$. The superior OFET performance of **S4** is also reflected in its threshold voltage (V_{th} = 12 V), which is lower than that of **P** (V_{th} = 32 V), and is possibly due to a lower density of trap sites in devices incorporating this material. We also note that trans-**S2** and **S3** have identical (within error) average mobilities of 1.1×10^{-2} $cm^2\ V^{-1}\ s^{-1}$, with on/off ratios of $\approx 2 \times 10^3$ and $\approx 2 \times 10^4$, respectively.

In an attempt to improve the mobility of **S4**, we thermally annealed the as-cast devices. This post-deposition treatment is a widely used method for promoting formation of ordered crystalline domains which are generally unable to form following the spin coating procedure. After annealing under an inert atmosphere for 20 min at 50 °C, we observed a 25-fold decrease in mobility ($\mu_e = 6.4 \times 10^{-3}$ $cm^2\ V^{-1}\ s^{-1}$) (see Figure S3, Supporting Information, for output and transfer characteristics). This was somewhat surprising given the thermal decomposition temperature of **S4** under a nitrogen atmosphere is 175 °C (95%), as measured by thermal gravimetric analysis (Figure S4, Supporting Information). Subsequent AFM analysis revealed that this loss of mobility is likely due to a higher proportion of well-defined grain boundaries that appear following thermal annealing, as discussed in Section 2.2. To avoid thermal treatment we subjected the as-cast film to solvent vapor annealing using $CHCl_3$, which has been shown to improve the crystallinity and electron mobility of the semiconducting layer in PDI based OFETs;[27] however, this led to discolouration of the semiconducting layer and gold electrodes and a subsequent decrease in mobility ($\mu_e = 8.7 \times 10^{-3}$ $cm^2\ V^{-1}\ s^{-1}$). While we were unable to improve the electron mobility by post-deposition treatment, the fact that the best performance was achieved using as-cast films of **S4** differentiates this material from the vast majority of PDI small molecule derivatives reported to date, which almost always require thermal deposition followed by post-deposition treatment to maximize electron mobility.

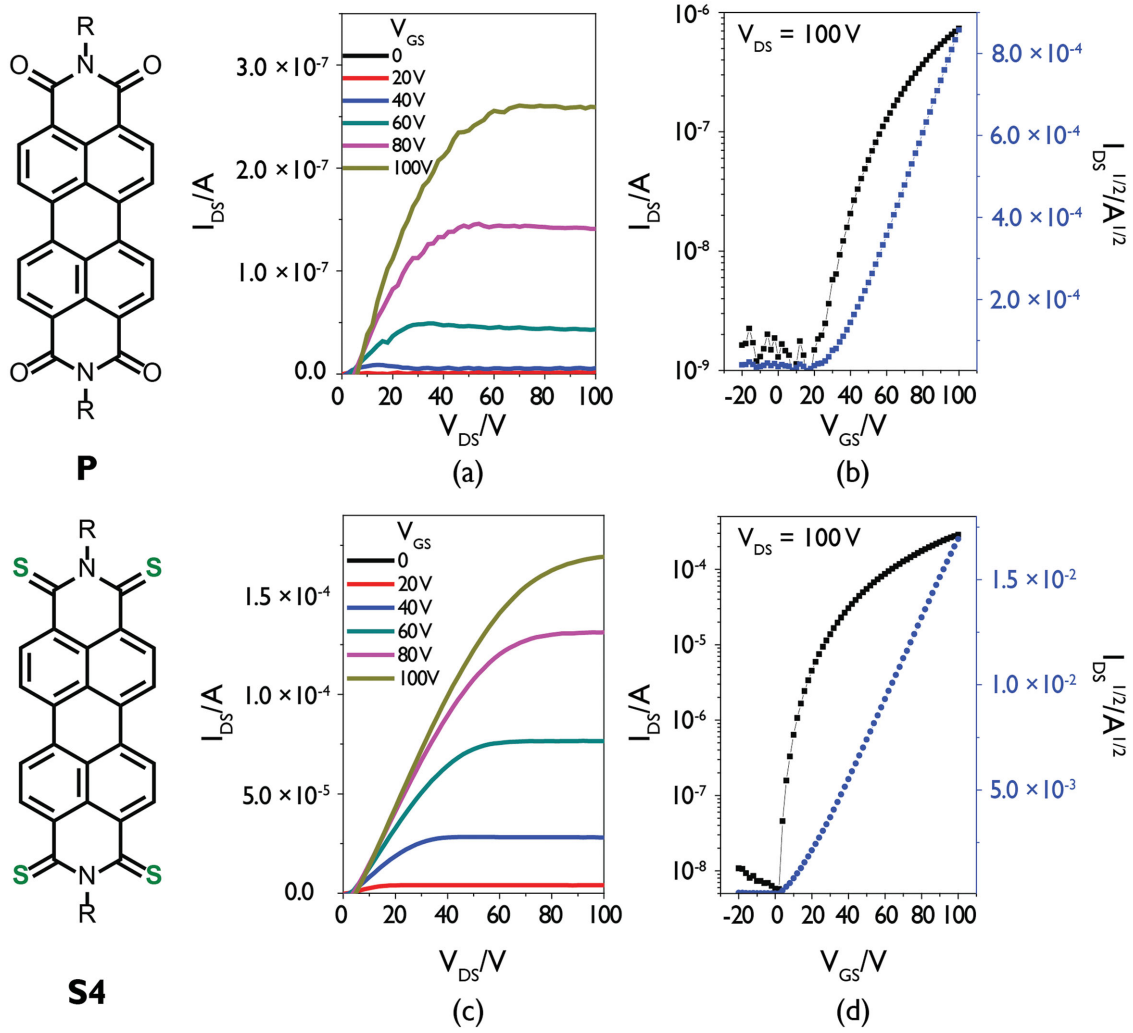

Figure 1. a,c) Output and b,d) transfer characteristics for the champion OFETs fabricated from **P** and **S4** on TDS-treated SiO_2 substrates. Chemical structures, output, and transfer characteristics of **S1**, ***trans*-S2**, and **S3** can be found in Figure S1, Supporting Information. The small shift of the onset current in the output curves likely results from leakage current between the drain and gate electrodes (see Figure S2, Supporting Information). R denotes the 3-hexylundecyl side-chain.

2.2. Solid-State Characterization

To begin our investigation of solid-state order in the films, we performed 2D wide angle X-ray scattering (2D-WAXS) experiments. The 2D detector employed collects a radial distribution of diffracted X-rays, allowing the molecular packing orientation and direction to be elucidated. For full experimental details refer to the Experimental Section. The 2D-WAXS experiments were conducted on films deposited on TDS-treated Si/SiO_2 substrates under identical solution deposition conditions as those used for the OFETs. The 1D X-ray diffraction patterns of films of each derivative (along the q_z direction) show an intense Bragg reflection at $2\theta = 3.57°$ (**P**), 3.54° (**S1**), 3.94° (***trans*-S2**), 3.60° (**S3**), and 3.48° (**S4**), corresponding to d-spacings of 24.74, 28.99, 26.05, 28.44, and 25.36 Å, respectively (**Figure 3** and Figure S4, Supporting Information). These reflections are indexed as (001) on the basis of their 2D diffraction images (see lower panels in Figure 3a,b), and are assigned to the interlayer spacing between planes of molecules oriented with their long axis parallel to the surface normal. While a precise determination of the molecular orientation at the surface cannot be obtained from these experiments, it is possible that the variation in d-spacings arise from slight differences in the

Table 1. Electron mobilities (μ_e), threshold voltages (V_{th}), and on/off ratios ($I_{on/off}$) for bottom contact OFET devices based on **P**-**S4**. The average mobility represents the average across five devices. Electron affinities were determined previously by cyclic voltammetry,[25] and are equal to the LUMO energy.

Compound	μ_e (avg.) [$cm^2\ V^{-1}\ s^{-1}$]	μ_e (max.) [$cm^2\ V^{-1}\ s^{-1}$]	$I_{on/off}$	V_{th} [V]	Electron affinity [eV]
P	6.9×10^{-4}	8.4×10^{-4}	$\approx 10^3$	32	−3.67
S1	3.9×10^{-3}	5.0×10^{-3}	$\approx 4 \times 10^3$	43	−3.80
***trans*-S2**	1.1×10^{-2}	2.6×10^{-2}	$\approx 2 \times 10^3$	40	−3.84
S3	1.1×10^{-2}	1.1×10^{-2}	$\approx 10^4$	8	−3.99
S4	0.16	0.19	$\approx 3 \times 10^3$	12	−4.12

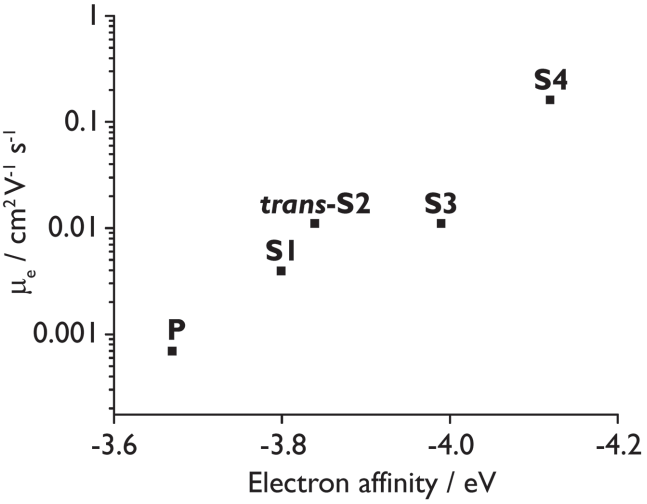

Figure 2. Electron affinity versus average electron mobility (μ_e) for **P**-**S4**. The mobilities were averaged across five devices.

tilt angle of the chromophores with respect to the surface, or through differences in their vertical displacement. We also note the higher intensity of the main Bragg reflection in **P**, which may indicate a higher degree of crystallinity in films of this material, although differences in film thickness makes the use of diffraction peak intensity as a means of assessing the relative degree of crystallinity challenging (see Figure 3 caption for relevant film thicknesses).

In the 2D diffraction images of the thionated derivatives there exist two symmetry-related reflections in the q_{xy} (in-plane) direction (see Figure 3 and Figure S4, Supporting Information) in addition to the main Bragg reflection in the q_z direction. In each case these reflections are of lower intensity than the q_z reflection and also have an identical d-spacing. These reflections are assigned to molecules packing face-on to the substrate surface (as discussed later in this section). Interestingly, we found that the intensity of the in-plane reflections increased (with respect to the main out-of-plane reflection) when the **S4** film was prepared by drop casting (see q_z:q_{xy} ratios in Figure S6, Supporting Information). This suggests that the molecular layers located at the top surface of the semiconductor films are comprised of molecules adopting a face-on orientation. We also note that the relative intensity of the in-plane reflections is higher in the ***trans*-S2**, **S3**, and **S4** derivatives, compared with **P** and **S1**. The possibility that this is related to differences in film thickness is ruled out on the basis that the spun cast film of **S4** is thinner than that of **S1** (41 vs 103 nm), confirming that a higher degree of thionation leads to a less isotropic crystallinity. The fact that the highest mobilities are achieved in the films containing a greater proportion of secondary crystalline phases suggests that these likely contribute to efficient long-range charge transport by providing multidirectional charge percolation pathways between the source and drain electrodes.

AFM was used to investigate the surface morphology of the films (**Figure 4**). AFM measurements were performed in tapping mode on films prepared under identical solution deposition conditions as the OFETs. In each of the films, a network-like morphology is observed. In the films of ***trans*-S2** and **S3**, there appear to be a larger number of 3D island structures than in films of **P** and **S1**, consistent with a greater propensity for aggregation in the more heavily thionated derivatives. This manifests as a higher surface roughness of these films (R_a = 20.2 and 16.0 nm, respectively). It is also noteworthy that the surface morphologies of **P** and **S4** are quite similar, with **S4** appearing to have larger domains and a higher surface roughness than **P** (19.7 vs 4.94 nm). This is likely due to aggregation promoted by stronger intermolecular London dispersion forces in **S4**, consistent with its higher calculated polarizability volume (see Table S1, Supporting Information).

In order to explain the loss of electron mobility in **S4** following thermal annealing (as noted earlier), we recorded AFM images of a film of **S4** pre- and post-annealing at 50 °C for 20 min in a nitrogen-filled glove box (Figure S8, Supporting Information). While the overall network-like morphology is maintained following thermal treatment, there appear to be discontinuities in the film morphology of the post-annealed film as evidenced by the emergence of island structures separated by well-defined grain boundaries. This morphological change is particularly evident in the corresponding phase images (see Figure S8, Supporting Information), and causes a slight increase in surface roughness of the film (15.8 to 16.6 nm). Similar island structures are observed in the as-cast films of trans-**S2** and **S3**, both of which have significantly lower electron mobilities than **S4**. The loss of mobility of **S4** following thermal annealing is thus likely due to the increased number of well-defined grain boundaries which act as trap sites that diminish charge transport.

It is well accepted that the charge accumulation layer in OFETs is located within the first few molecular layers above the gate dielectric.[28] Thus, in order to understand how film morphology varies with film thickness, we performed AFM measurements on films of **P** and **S4** which were prepared by spin coating from 5 and 10 mg mL^{-1} chloroform solutions. Solution deposition was used to vary the film thickness since this is consistent with the device fabrication conditions employed, thus allowing us to better correlate morphology to device performance. In order to smoothen the films and reveal greater morphological detail, the casting solutions were drop cast onto the TDS-treated Si/SiO_2 substrate while it was rapidly spinning (see the Experimental Section for details).[29] This resulted in films of **P** with thicknesses of 27 nm (5 mg mL^{-1}) and 56 nm (10 mg mL^{-1}), and R_a (roughness) factors of 1.34 and 2.95 nm, respectively. Attempts at preparing thinner films using more dilute casting solution concentrations led to nonuniform surface coverage. Given that molecules of **P** align with their long axis edge-on to the substrate surface (as revealed in the 2D-WAXS experiments), a thickness of 27 nm corresponds to ≈8–10 molecular layers, if no side-chain interdigitation occurs. The large difference in thickness of the 5 and 10 mg mL^{-1} films of **P** is expected due to the solely edge-on molecular packing adopted, which would make film thickness more sensitive to casting solution concentration. In contrast, the thicknesses of the **S4** films cast from the 5 and 10 mg mL^{-1} solutions are only marginally different (33 and 36 nm, respectively), suggesting that the additional crystalline phases observed in the 2D-WAXS experiments of the thionated derivatives could correspond to

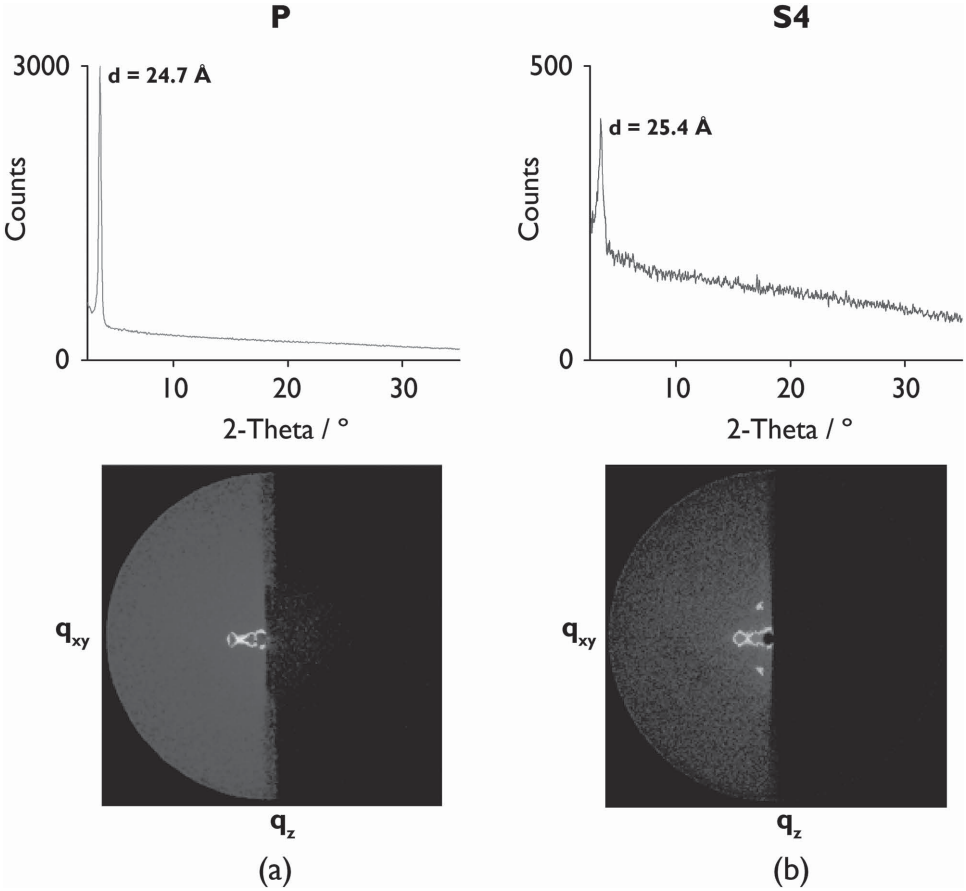

Figure 3. a,b) X-ray diffraction patterns of thin films of **P** and **S4** on TDS-treated SiO_2 substrates along the q_z (out-of-plane) packing direction. The lower panels show the corresponding 2D-WAXS diffraction frame image. The film thicknesses are 59 nm (**P**) and 40 nm (**S4**). While **P** and **S4** appear to be crystalline, the reflections observed in the q_{xy} (in-plane) direction in the frame image of **S4** suggest the presence of additional crystalline phases in films of this material.

layers of molecules stacking face-on to the substrate. The different crystalline phases present in films of **S4** make it difficult to determine the precise number of molecular layers stacked atop the Si/SiO_2 substrate. Nevertheless, we are able to gain an initial understanding as to how morphology varies with film thickness in films of **P** and **S4**.

AFM height images of the 5 mg mL^{-1} films show a similar network-like morphology as for the films of **P** and **S4** cast from 10 mg mL^{-1} solutions (**Figure 5**), although the domain sizes appear to have become smaller. The film of **S4** cast from the 5 mg mL^{-1} solution appears to have larger domain sizes and more continuous grain boundaries than the film of **P** prepared under the same conditions (see also Figure S10, Supporting Information). This would be expected to aid long range charge transport by providing more continuous charge transport pathways across grain boundaries.[30] More continuous grain boundaries are also evident in the 10 mg mL^{-1} film of **S4** (Figure S10, Supporting Information), suggesting that this could be a general feature of thin films of this compound. This, in addition to the additional charge percolation pathways in films of **S4** revealed in the 2D-WAXS experiments, is expected to contribute to the higher electron mobility of this derivative.

2.3. Modeling Charge Transport Efficiency

In order to investigate the efficiency of electron transfer in the PDIs, we compared the electronic coupling matrix elements for electron (V_L) and hole transfer (V_H) within molecular dimers using Koopmans' theorem (also called the symmetric dimer splitting method).[31] In this approach, the coupling interaction between the frontier highest occupied molecular orbital (HOMO) and LUMO of the constituent chromophores within a noncovalently bound molecular dimer splits them into a mixture of symmetric and anti-symmetric combinations. The electronic coupling matrix element for electrons (holes) is then calculated as the absolute value of half the energy difference between the LUMO (HOMO) and LUMO+1 (HOMO-1) orbitals. One drawback of Koopmans' theorem is that it neglects the reorganization energy which is implicit in the Marcus theory description of electron transfer.[32] While self-consistent field methods which take into account the reorganization energy might be expected to yield more reliable results, the reorganization energy is not expected to vary significantly across the series of PDIs due to their nearly identical molecular geometries and the expected similarities in the energies of the nuclear vibrational modes within the reactant and product

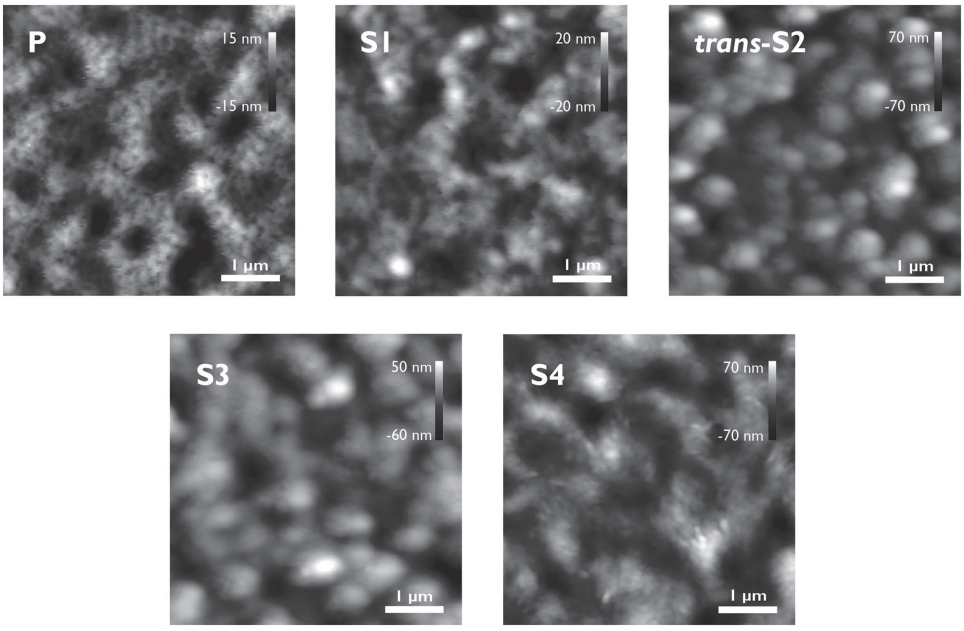

Figure 4. AFM height images of **P**-**S4** taken on TDS-treated SiO_2 substrates. The corresponding phase images are shown in Figure S7, Supporting Information. Film thicknesses are 59 nm (**P**), 103 nm (**S1**), 108 nm (***trans*-S2**), 73 nm (**S3**), and 40 nm (**S4**), as determined by profilometry.

potential energy surfaces. Thus the reorganization energy can be safely neglected in these calculations.

The calculations were performed using the M06–2X hybrid exchange-correlation functional with the 6–31++g(d,p) basis set,[33] and by applying the basis set superposition error (BSSE) correction of Boys and Bernardi for calculating the binding energies of the molecular dimers.[34] The M06–2X functional was chosen due to the ability of the M06 family of functionals

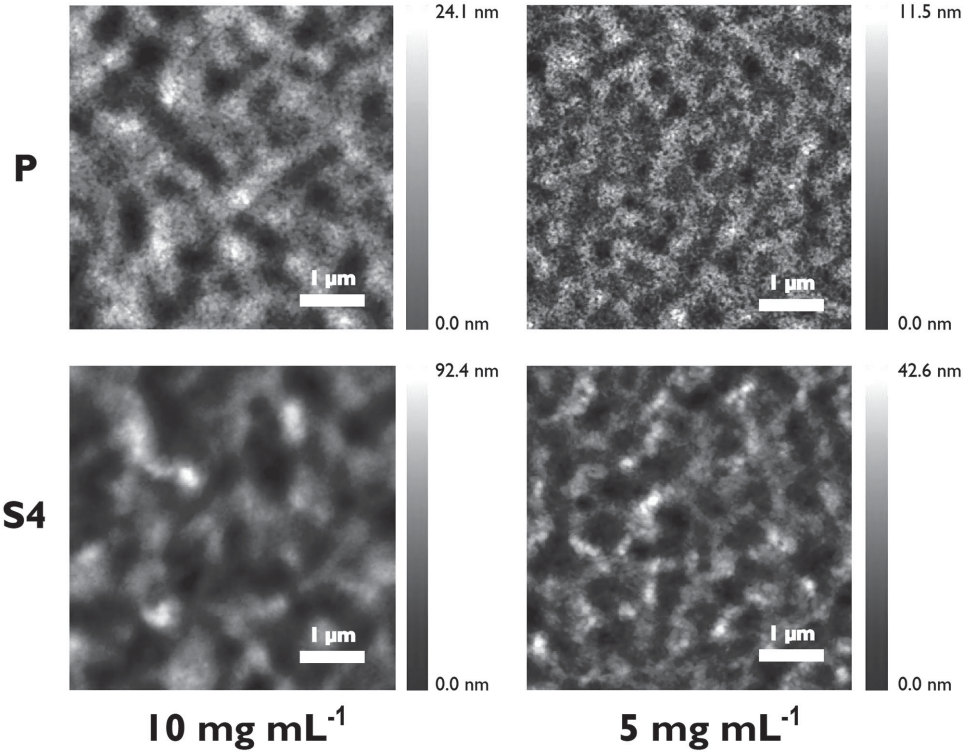

Figure 5. AFM height images of **P**-**S4** taken on TDS-treated SiO_2 substrates from 10 and 5 mg mL^{-1} casting solutions. The corresponding phase images are shown in Figure S9, Supporting Information. The 10 mg mL^{-1} films are smoother than the corresponding films shown in Figure 4 due to the different spin coating conditions used.

Table 2. Calculated electronic coupling matrix elements (V_L and V_H), and BSSE-corrected binding energies for **P**-**S4**. A longitudinal displacement of 1.5 Å has been applied. Calculations were performed using the M06–2X functional and 6–31++g(d,p) basis set.

Compound	V_L [eV]	V_H [eV]	Binding energy [kcal mol^{-1}]
P	0.22	0.06	20.1
S1	0.23	0.03	21.4
***trans*-S2**	0.23	0.02	22.8
S3	0.25	0.03	24.3
S4	0.26	0.01	25.6

to satisfactorily account for "medium-range" (<5 Å) dispersion interactions in noncovalent complexes. Indeed, this functional has been successively used for mapping binding energies and electronic coupling matrix elements in a π–π stacked PDI dimer,[35] and has proven more accurate than the dispersion-corrected PBE-D functional of Perdew, Burke, and Wang for applications such as calculating π–π interactions between nucleic acid base pairs in biomacromolecules.[36]

For determination of V_L and V_H the optimized geometry of each derivative was first calculated at the M06–2X/6–31++g(d,p) level of theory under tight convergence criteria. In each case the 3-hexylundecyl side-chains were replaced with a single hydrogen atom to minimize computational demand. A cofacially stacked molecular dimer was then constructed using a fixed interchromophore separation of 3.5 Å. This value was chosen as it lies within the range of π–π stacking distances typically found for noncore functionalized PDI derivatives (3.3–3.5 Å).[37] To determine the lowest energy dimer configuration, the molecules were longitudinally displaced in 0.5 Å increments and the binding energies calculated at each increment. This process was repeated until a total displacement (L) of 5.0 Å had been reached. To minimize computational time, lateral (short-axis) displacements were not considered.

For each derivative the highest binding energy is obtained when L = 1.5 Å, which thus corresponds to the optimal dimer configuration. As the degree of thionation increases the binding energies at each L become progressively larger, suggesting that noncovalent π–π interactions are enhanced by oxygen–sulfur atomic substitution (see Figure S11 and Table S2, Supporting Information). This is expected due to the increase in the calculated polarizability volume with degree of thionation (see Table S1, Supporting Information), leading to stronger intermolecular London dispersion forces, and is consistent with solution phase ^{1}H NMR binding studies on **P** and **S4** which showed stronger π–π interactions in **S4** than in **P**.[25] At the optimized geometry (L = 1.5 Å), V_L becomes progressively larger with degree of thionation such that **S4** has the highest matrix element for electron transfer (0.26 eV) (**Table 2**). Indeed, V_L is calculated to be higher than V_H at every longitudinal displacement considered, except when 2.0 < L < 3.0 Å. The optimal dimer geometry also represents the configuration in which V_H is at its minimum value (for the thionated derivatives). V_H is, in fact, an order of magnitude lower than V_L for each of **S1**–**S4** at the optimal dimer configuration, consistent with the n-type behavior of thionated PDIs observed in the OFETs (assuming the dimer structures are representative of local intermolecular order in the devices). It is also apparent that for each derivative V_H is larger than V_L when L = 2.5 Å, indicating that in this dimer configuration hole transport is expected to be more efficient. This suggests that thionated PDIs may display ambipolar charge mobility in certain molecular packing arrangements. Significantly, a strong positive correlation between V_L and average electron mobility (μ_e) is found (**Figure 6**b), suggesting that more efficient intermolecular electron transport contributes to the observed increase in electron mobility with degree of thionation.

3. Conclusion

This work has demonstrated the power of oxygen–sulfur atomic substitution to enhance the electron mobility of a bis-*N*-alkylated PDI derivative. Using a combination of solid state characterization techniques and density functional calculations, we showed that the positive correlation observed between electron mobility and degree of thionation can be attributed to a combination of solid state properties and local intermolecular interactions that are enhanced by oxygen–sulfur substitution.

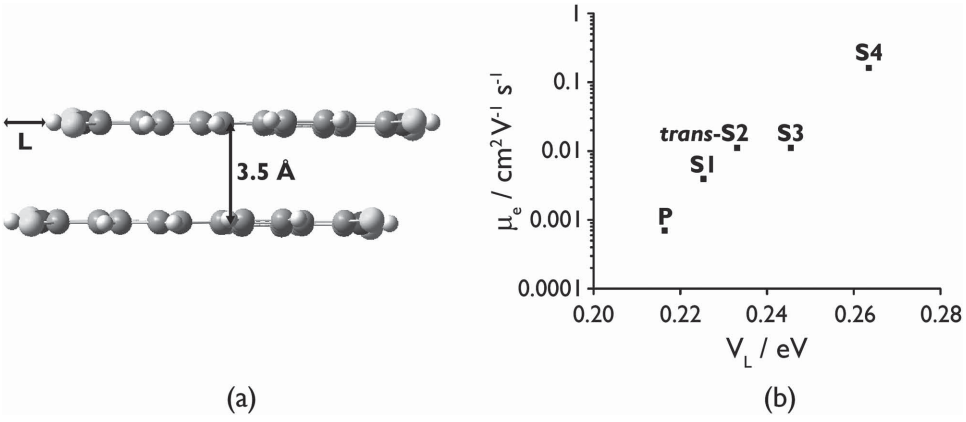

Figure 6. a) Structure of the optimized **S4** dimer (L = 1.5 Å), and b) a plot of the electronic coupling matrix elements for electron transfer (V_L) for each derivative versus average electron mobility (μ_e) when L = 1.5 Å.

X-ray diffractograms of the device active layers showed that all the PDIs stack edge-on to the substrate with their long molecular axis parallel to the surface normal. In films of the thionated derivatives we were able to observe additional Bragg reflections from the presence of orthogonal crystalline phases, which likely promote multidirectional charge transport in devices of these derivatives. Films of the more heavily thionated derivatives (***trans*-S2–S4**) were found to have the greatest proportion of these orthogonal crystalline phases. AFM imaging revealed a similar network-like morphology in the films of each derivative. In the thinner films of **P** and **S4** slight differences in morphology were observed, including more continuous grain boundaries in **S4**, which likely contributes to its higher mobility.

Density functional calculations on molecular dimers showed that each derivative displays n-type behavior at the optimal dimer configuration. A strong positive correlation between electron mobility and electron transfer efficiency was observed at the optimal dimer configuration, suggesting that more efficient intermolecular electron transfer contributes to the increase in electron mobility with degree of thionation.

This work has shown that thionated PDIs are highly promising n-type materials for organic electronics. Significantly, the high electron mobility of **S4** (0.16 $cm^2\ V^{-1}\ s^{-1}$) was achieved from solution cast films without the need for post-deposition treatment, which represents a distinct advantage over the majority of PDI-based OFETs reported to date. This work thus sets the stage for the development of new thionated PDI derivatives for high performance organic electronics applications.

4. Experimental Section

TDS was purchased from Sigma-Aldrich and used as received. 2D wide angle X-ray scattering data was collected at McMaster University (Hamilton, ON, Canada) on a Bruker D8 DISCOVER with DAVINCI. DESIGN using a Cobalt Sealed Tube Source (λ_{avg} = 1.79026 Å) and a Vantec 500 (MikroGap TM Technology) area detector. An incidence angle of 1.0° was used. Collected 2D frames were integrated into intensity versus 2-theta plots using DIFFRAC.EVA Version 3.0 software. To enable comparability, samples for XRD were prepared under identical conditions as the OFETs. AFM imaging was conducted in tapping mode on a Veeco Dimension 3000 microscope, or on a Bruker Dimension Icon Atomic Force Microscope. AFM was performed on the films used for the 2D-WAXS experiments. Thinner films of **P** and **S4** for AFM were fabricated from 5 mg mL^{-1} chloroform solutions, and deposited by drop casting the solution onto the TDS-treated Si/SiO_2 substrate while it was rotating at 3000 rpm.[29] Spinning was continued for a further 30 s at 3000 rpm, before allowing the films to dry under ambient conditions and in the dark for at least 1 h prior to imaging. Film thicknesses were measured using a KLA-Tencor P16+ stylus profiler across a mechanical scratch applied to the film.

The semiconducting performance of the PDIs was characterized by a bottom-gate, bottom-contact OFET structure (W = 1 mm; L = 30 µm, W/L = 33). A heavily n-doped Si wafer with a 300 nm thick SiO_2 layer was used as the substrate, where the conductive Si layer and the SiO_2 layer function as the gate and dielectric, respectively. The source/drain electrode pairs were prepared by thermal evaporation of gold through a shadow mask. The substrates were cleaned using an ultrasonic bath with deionized (DI) water, rinsed with acetone and isopropanol, and then immersed in a TDS solution (3% in toluene) for 15 min. The semiconducting films with a thickness of ≈30–50 nm were deposited on the substrate by spin coating 10 mg mL^{-1} solutions of **S1**–**S4** in chloroform at 3000 rpm for 60 s, followed by heating at 30 °C for 20 min to remove the solvent. **P** was deposited using a spin speed of 6000 rpm. All measurements were performed in a nitrogen atmosphere in the absence of light by an Agilent B2912A Semiconductor Analyzer. The electron mobility (μ_e), threshold voltage (V_{th}), and current on/off ratio ($I_{on/off}$) of each device were determined from the drain–source current (I_{DS}) versus gate–source voltage (V_{GS}) plots using the standard field effect transistor equations.[38] All calculations were performed using the Gaussian09 software package (see the Supporting Information for full Gaussian citation and additional computational details).

Supporting Information

Supporting information is available from the Wiley Online Library or from the author.

Acknowledgements

This work was supported by NSERC, DuPont, and the A. P. Sloan Foundation. The authors would like to thank Victoria Jarvis (McMaster University) for recording the 2D-WAXS data. A.J.T. would like to thank the Connaught Global Challenge Award for a postdoctoral fellowship. M.B.M. is grateful for an Ontario Graduate Scholarship. T.B.S. is grateful for a graduate scholarship (NSERC-PGS).

Received: March 2, 2015
Revised: March 30, 2015
Published online: April 17, 2015

[1] a) A. Facchetti, *Mater. Today* **2007**, *10*, 28; b) M. M. Payne, S. R. Parkin, J. E. Anthony, C.-C. Kuo, T. N. Jackson, *J. Am. Chem. Soc.* **2005**, *127*, 4986.

[2] a) H. E. Katz, A. J. Lovinger, J. Johnson, C. Kloc, T. Siegrist, W. Li, Y.-Y. Lin, A. Dodabalapur, *Nature* **2000**, *404*, 478; b) A. Babel, S. A. Jenekhe, *J. Am. Chem. Soc.* **2003**, *125*, 13656; c) P. Wei, J. H. Oh, G. Dong, Z. Bao, *J. Am. Chem. Soc.* **2010**, *132*, 8852; d) M. M. Ling, P. Erk, M. Gomez, M. Koenemann, J. Locklin, Z. Bao, *Adv. Mater.* **2007**, *19*, 1123; e) H. Yan, Z. Chen, Y. Zheng, C. Newman, J. R. Quinn, F. Dötz, M. Kastler, A. Facchetti, *Nature* **2009**, *457*, 679.

[3] a) F. Nolde, W. Pisula, S. Müller, C. Kohl, K. Müllen, *Chem. Mater.* **2006**, *18*, 3715; b) E. Kozma, M. Catellani, *Dyes Pigm.* **2013**, *98*, 160; c) C. E. Finlayson, R. H. Friend, M. B. J. Otten, E. Schwartz, J. J. L. M. Cornelissen, R. J. M. Nolte, A. E. Rowan, P. Samorì, V. Palermo, A. Liscio, K. Peneva, K. Müllen, S. Trapani, D. Beljonne, *Adv. Funct. Mater.* **2008**, *18*, 3947; d) G. R. J. Müller, C. Meiners, V. Enkelmann, Y. Geerts, K. Müllen, *J. Mater. Chem.* **1998**, *8*, 61; e) C. Huang, S. Barlow, S. R. Marder, *J. Org. Chem.* **2011**, *76*, 2386; f) T. E. Kaiser, V. Stepanenko, F. Würthner, *J. Am. Chem. Soc.* **2009**, *131*, 6719; g) K. Balakrishnan, A. Datar, T. Naddo, J. Huang, R. Oitker, M. Yen, J. Zhao, L. Zang, *J. Am. Chem. Soc.* **2006**, *128*, 7390.

[4] a) E.-F. Huo, Y. Zou, H.-Q. Sun, J.-L. Bai, Y. Huang, Z.-Y. Lu, Y. Liu, Q. Jiang, S.-L. Zhao, *Polym. Bull.* **2011**, *67*, 843; b) E. Zhou, J. Cong, Q. Wei, K. Tajima, C. Yang, K. Hashimoto, *Angew. Chem. Int. Ed.* **2011**, *50*, 2799; c) Y. Liu, T. T. Larsen-Olsen, X. Zhao, B. Andreasen, R. R. Søndergaard, M. Helgesen, K. Norrman, M. Jørgensen, F. C. Krebs, X. Zhan, *Sol. Energy Mater. Sol. Cells* **2013**, *112*, 157.

[5] L. M. Kozycz, D. Gao, A. J. Tilley, D. S. Seferos, *J. Polym. Sci. Part A: Polym. Chem.* **2014**, *52*, 3337.

[6] a) Y. Li, L. Xu, T. Liu, Y. Yu, H. Liu, Y. Li, D. Zhu, *Org. Lett.* **2011**, *13*, 5692; b) X. Feng, F. Feng, M. Yu, F. He, Q. Xu, H. Tang, S. Wang, Y. Li, D. Zhu, *Org. Lett.* **2008**, *10*, 5369; c) W. Jiang, Y. Li, W. Yue, Y. Zhen, J. Qu, Z. Wang, *Org. Lett.* **2010**, *12*, 228.

[7] a) Q. Yan, Y. Zhou, Y. Zheng, J. Pei, D. Zhao, *Chem. Sci.* **2013**, *4*, 4389; b) X. Zhang, Z. Lu, L. Ye, C. Zhan, J. Hou, S. Zhang, B. Jiang, Y. Zhao, J. Huang, S. Zhang, Y. Liu, Q. Shi, Y. Liu, J. Yao, *Adv. Mater.* **2013**, *25*, 5791; c) Y. Lin, Y. Wang, J. Wang, J. Hou, Y. Li, D. Zhu, X. Zhan, *Adv. Mater.* **2014**, *26*, 5137.

[8] a) B. A. Llewellyn, A. G. Slater, G. Goretzki, T. L. Easun, X.-Z. Sun, E. S. Davies, S. P. Argent, W. Lewis, A. Beeby, M. W. George, N. R. Champness, *Dalton Trans.* **2014**, *43*, 85; b) Á. J. Jiménez, F. Spänig, M. S. Rodríguez-Morgade, K. Ohkubo, S. Fukuzumi, D. M. Guldi, T. Torres, *Org. Lett.* **2007**, *9*, 2481; c) A. Prodi, C. Chiorboli, F. Scandola, E. Iengo, E. Alessio, R. Dobrawa, F. Würthner, *J. Am. Chem. Soc.* **2005**, *127*, 1454; d) A. A. Rachford, S. Goeb, F. N. Castellano, *J. Am. Chem. Soc.* **2008**, *130*, 2766.

[9] a) A. Sharenko, C. M. Proctor, T. S. van der Poll, Z. B. Henson, T.-Q. Nguyen, G. C. Bazan, *Adv. Mater.* **2013**, *25*, 4403; b) R. Singh, E. Aluicio-Sarduy, Z. Kan, T. Ye, R. C. I. MacKenzie, P. E. Keivanidis, *J. Mater. Chem. A* **2014**, *2*, 14348; c) V. Kamm, G. Battagliarin, I. A. Howard, W. Pisula, A. Mavrinskiy, C. Li, K. Müllen, F. Laquai, *Adv. Energy Mater.* **2011**, *1*, 297.

[10] a) P. J. Jadhav, P. R. Brown, N. Thompson, B. Wunsch, A. Mohanty, S. R. Yost, E. Hontz, T. Van Voorhis, M. G. Bawendi, V. Bulović, M. A. Baldo, *Adv. Mater.* **2012**, *24*, 6169; b) P. D. Reusswig, D. N. Congreve, N. J. Thompson, M. A. Baldo, *Appl. Phys. Lett.* **2012**, *101*, 113304.

[11] a) S. W. Eaton, L. E. Shoer, S. D. Karlen, S. M. Dyar, E. A. Margulies, B. S. Veldkamp, C. Ramanan, D. A. Hartzler, S. Savikhin, T. J. Marks, M. R. Wasielewski, *J. Am. Chem. Soc.* **2013**, *135*, 14701; b) N. Renaud, P. A. Sherratt, M. A. Ratner, *J. Phys. Chem. Lett.* **2013**, *4*, 1065.

[12] a) S. Schols, S. Verlaak, C. Rolin, D. Cheyns, J. Genoe, P. Heremans, *Adv. Funct. Mater.* **2008**, *18*, 136; b) D. Liu, H. Ren, J. Li, Q. Tao, Z. Gao, *Chem. Phys. Lett.* **2009**, *482*, 72.

[13] a) X. Zhan, A. Facchetti, S. Barlow, T. J. Marks, M. A. Ratner, M. R. Wasielewski, S. R. Marder, *Adv. Mater.* **2011**, *23*, 268; b) A. L. Briseno, S. C. B. Mannsfeld, C. Reese, J. M. Hancock, Y. Xiong, S. A. Jenekhe, Z. Bao, Y. Xia, *Nano Lett.* **2007**, *7*, 2847.

[14] Z. Liu, G. Zhang, Z. Cai, X. Chen, H. Luo, Y. Li, J. Wang, D. Zhang, *Adv. Mater.* **2014**, *26*, 6965.

[15] F. Würthner, M. Stolte, *Chem. Commun.* **2011**, *47*, 5109.

[16] J. Rivnay, L. H. Jimison, J. E. Northrup, M. F. Toney, R. Noriega, S. Lu, T. J. Marks, A. Facchetti, A. Salleo, *Nat. Mater.* **2009**, *8*, 952.

[17] R. T. Weitz, K. Amsharov, U. Zschieschang, E. B. Villas, D. K. Goswami, M. Burghard, H. Dosch, M. Jansen, K. Kern, H. Klauk, *J. Am. Chem. Soc.* **2008**, *130*, 4637.

[18] F. Würthner, P. Osswald, R. Schmidt, T. E. Kaiser, H. Mansikkamaki, M. Konemann, *Org. Lett.* **2006**, *8*, 3765.

[19] M. Gsänger, J. H. Oh, M. Könemann, H. W. Höffken, A.-M. Krause, Z. Bao, F. Würthner, *Angew. Chem. Int. Ed.* **2010**, *49*, 740.

[20] Z. Yuan, J. Li, Y. Xiao, Z. Li, X. Qian, *J. Org. Chem.* **2010**, *75*, 3007.

[21] a) J. H. Oh, Y. Sen Sun, R. Schmidt, M. F. Toney, D. Nordlund, M. Könemann, F. Würthner, Z. Bao, *Chem. Mater.* **2009**, *21*, 5508; b) J. H. Oh, S. Liu, Z. Bao, R. Schmidt, F. Würthner, *Appl. Phys. Lett.* **2007**, *91*, 212107; c) H. Chen, M. Ling, X. Mo, M. Shi, M. Wang, Z. Bao, *Chem Mater.* **2007**, *19*, 816; d) R. Schmidt, J. H. Oh, Y. Sen Sun, M. Deppisch, A. M. Krause, K. Radacki, H. Braunschweig, M. Könemann, P. Erk, Z. Bao, F. Würthner, *J. Am. Chem. Soc.* **2009**, *131*, 6215; e) M.-M. Shi, H.-Z. Chen, J.-Z. Sun, J. Ye, M. Wang, *Chem. Commun.* **2003**, 1710; f) H. Z. Chen, M. M. Shi, T. Aernouts, M. Wang, G. Borghs, P. Heremans, *Sol. Energy Mater. Sol. Cells* **2005**, *87*, 521.

[22] L. Ma, Y. Guo, Y. Wen, Y. Liu, X. Zhan, *Appl. Phys. Lett.* **2013**, *103*, 203303.

[23] a) R. J. Chesterfield, J. C. McKeen, C. R. Newman, P. C. Ewbank, D. A. da Silva Filho, J.-L. Brédas, L. L. Miller, K. R. Mann, C. D. Frisbie, *J. Phys. Chem. B* **2004**, *108*, 19281; b) S. Tatemichi, M. Ichikawa, T. Koyama, Y. Taniguchi, *Appl. Phys. Lett.* **2006**, *89*, 112108.

[24] X. Zhan, A. Facchetti, S. Barlow, T. J. Marks, M. A. Ratner, M. R. Wasielewski, S. R. Marder, *Adv. Mater.* **2011**, *23*, 268.

[25] A. J. Tilley, R. D. Pensack, T. S. Lee, B. Djukic, G. D. Scholes, D. S. Seferos, *J. Phys. Chem. C* **2014**, *118*, 9996.

[26] L.-L. Chua, J. Zaumseil, J.-F. Chang, E. C.-W. Ou, P. K.-H. Ho, H. Sirringhaus, R. H. Friend, *Nature* **2005**, *434*, 194.

[27] R. C. Savage, E. Orgiu, J. M. Mativetsky, W. Pisula, T. Schnitzler, C. L. Eversloh, C. Li, K. Müllen, P. Samorì, *Nanoscale* **2012**, *4*, 2387.

[28] a) B. Park, A. Aiyar, J. Hong, E. Reichmanis, *ACS Appl. Mater. Interfaces* **2011**, *3*, 1574; b) H. G. O. Sandberg, G. L. Frey, M. N. Shkunov, H. Sirringhaus, R. H. Friend, M. M. Nielsen, C. Kumpf, *Langmuir* **2002**, *18*, 10176.

[29] F. Zhang, C. Di, N. Berdunov, Y. Hu, Y. Hu, X. Gao, Q. Meng, H. Sirringhaus, D. Zhu, *Adv. Mater.* **2013**, *25*, 1401.

[30] a) S. Verlaak, V. Arkhipov, P. Heremans, *Appl. Phys. Lett.* **2003**, *82*, 745; b) Z. Bao, A. Lovinger, A. Dodabalapur, *Appl. Phys. Lett.* **1996**, *69*, 3066; c) R. J. Kline, M. D. McGehee, E. N. Kadnikova, J. Liu, J. M. J. Fréchet, M. F. Toney, *Macromolecules* **2005**, *38*, 3312; d) W. Shi, S. Han, W. Huang, J. Yu, *Appl. Phys. Lett.* **2015**, *106*, 043303.

[31] T. Koopmans, *Physica* **1934**, *1*, 104.

[32] J.-L. Brédas, D. Beljonne, V. Coropceanu, J. Cornil, *Chem. Rev.* **2004**, *104*, 4971.

[33] Y. Zhao, D. G. Truhlar, *Theor. Chem. Acc.* **2008**, *120*, 215.

[34] S. F. Boys, F. Bernardi, *Mol. Phys.* **1970**, *19*, 553.

[35] J. Vura-Weis, M. A. Ratner, M. R. Wasielewski, *J. Am. Chem. Soc.* **2010**, *132*, 1738.

[36] a) J. P. Perdew, K. Burke, M. Ernzerhof, *Phys. Rev. Lett.* **1996**, *77*, 3865; b) E. G. Hohenstein, S. T. Chill, C. D. Sherrill, *J. Chem. Theory Comput.* **2008**, *4*, 1996.

[37] a) E. Hädicke, F. Graser, *Acta Crystallogr. Sect. C: Cryst. Struct. Commun.* **1986**, *42*, 189; b) E. Hädicke, F. Graser, *Acta Crystallogr. Sect. C: Cryst. Struct. Commun.* **1986**, *42*, 195; c) P. Zugenmaier, J. Duff, T. Bluhm, *Cryst. Res. Technol.* **2000**, *35*, 1095.

[38] V. Coropceanu, J. Cornil, D. A. da Silva Filho, Y. Olivier, R. Silbey, J.-L. Brédas, *Chem. Rev.* **2007**, *107*, 926.